2009 IEEE International Conference on Robotics and Automation
Kobe International Conference Center
Kobe, Japan, May 12-17, 2009

Mechanics of Bending, Torsion, and Variable Precurvature in Multi-Tube Active Cannulas

D. Caleb Rucker and Robert J. Webster III
Vanderbilt University, Department of Mechanical Engineering, Nashville, Tennessee, USA

Abstract— **Active cannulas are a relatively new continuum robot subclass characterized by their use of preshaped tubes that transmit bending moments as they slide within one another and are axially rotated. Previous (experimentally vetted) mechanics-based models of active cannula shape assume piecewise constant precurvature of component tubes, and neglect torsion in curved sections of the device. Recently a general, coordinate-free, energy-based framework for active cannula shape has been formulated that relaxes these requirements and includes all prior models as special cases. However, only the 2-tube, constant-precurvature case has thus far been explored in detail using the framework. In this paper we consider the general case of an arbitrary number of component tubes and precurvatures that vary with arc length, deriving a set of differential equations that capture both bending and torsional effects continuously along the active cannula backbone. We then show how to solve these differential equations numerically to describe active cannula shape.**

I. Introduction

Tentacle-like continuum robots with elastic backbones can reach dexterously through cluttered or geometrically constrained environments, and offer a number of potential advantages over traditional rigid-link robots [15]. Active cannulas are a type of continuum robot consisting of preshaped elastic tubes. These tubes are concentric and are differentially extended and rotated at their respective bases to generate dexterity (see Figure 1). These robots use the component tubes within their backbones to transmit bending moments, rather than the support disks actuated by tendon wires [3], [6], flexible push rods, [14], or pneumatic actuators [2], [7] that are used in larger-scale continuum robot designs. While building bending actuation directly into the backbone permits small diameters, one potential drawback is an increase in modeling complexity, since all arcs and curves in the backbone will be coupled through tube elastic interaction.

Motivation for developing active cannulas despite the challenge of modeling these effects comes from their potential in minimally invasive surgery and other tasks that require thin, dexterous manipulators. Active cannulas have been proposed for biopsy or treatment of lung lesions through the throat [20], transgastric abdominal surgery [18], fetal procedures [5], steering needles embedded in tissue, [8], [13], cardiac procedures [13], and transnasal skull base access [18] – see [16] for an overview of possible medical applications. Some of the above applications require passage through air-filled cavities (e.g. lung), where free-space kinematic models such as the one derived in this paper will apply directly. Others involve passage through soft tissues, where free-space models serve as a starting point for augmented models

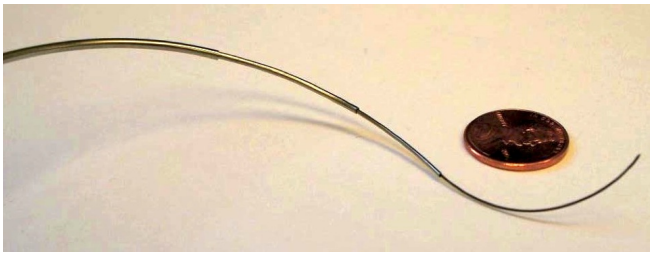

Fig. 1. A prototype active cannula made of four superelastic nitinol tubes and one central wire (with three tubes and the wire visible).

that include tissue interaction effects. Conceptually, such augmented models may be derived in a similar manner to what has previously been done for needles that steer through soft tissue based on tip geometry or base actuation (see e.g. [1], [4], [17], or [16] for an overview). Thus, both free-space and tissue-embedded applications will require an accurate kinematic model of active cannula shape, which motivates our work.

Models of active cannula shape have evolved over the past few years, continually increasing in generality and predictive power. The simplest model treats each outer tube as infinitely rigid (in both bending and torsion) compared to all those within it [5], reducing kinematics to the geometric task of describing transformations along a piecewise circular robot. In this case, a number of formulations exist, including [6]. However, experiments have revealed that elastic tubes generally interact significantly, causing one another to bend. Modeling this effect via Bernoulli-Euler beam mechanics leads to a significant improvement in model accuracy [8], [13], [18]. A more recent discovery is that active cannula shape also strongly depends on the effect of torsion. Including torsion in even a limited sense (in the initial straight transmission only) has been shown to further enhance model accuracy, and also structurally enable prediction of experimentally observed instabilities (bifurcations) as the energy landscape changes with variation in the translations and rotations input at tube bases [20].

Torsion in curved sections of concentric curved tubes was first included in [11], which considered a 2-tube, circularly precurved active cannula, deriving a differential equation for the difference in axial 'twist' angles along the tubes. This general inclusion of torsion improved accuracy by 72% with respect to a pure bending model and 35% in comparison to the transmissional torsion model [20], in a set of experiments. These results indicated the need for a general framework

that accounts for bending and torsion throughout a cannula with more than two tubes, which was derived in [12], but only fully explored in the 2-tube, circularly precurved case. In [12], it was also shown that the new framework can reduce to any of the prior models referenced above, provided appropriate assumptions are applied.

The new modeling framework [12] has the potential to greatly expand the capabilities of active cannulas, enabling them to attain complex desired curvature functions with significantly fewer tubes, and to deploy through more complex trajectories. Such capabilities will be particularly important for enabling 'patient specific' cannulas whose deployment trajectories are defined using medical images. It is likely that variable (non-circular) precurvature functions and more than two tubes will be required to achieve many of these trajectories. The work in this paper addresses these challenges. We derive a system of differential equations describing the shape of an arbitrarily large collection of tubes with general precurvature functions. We then solve this system of equations numerically to compute overall cannula shape. These results are derived within a general beam-mechanics-based framework (reviewed in Section II), which has been experimentally supported in [13], [16], [19]–[21].

II. Review of Modeling Framework

For reader convenience, we provide a brief review of the active cannula forward kinematic model derived in [12], which is an extension of the framework given in [11], [20]. The basic strategy employed is that of minimizing the total elastic energy stored in a collection of n preshaped tubes to yield the equilibrium conformation of the cannula.

Let each preset tube shape be defined by a curve through space $p_i^*(s)$, where $s \in [0, \ell]$ is the arc length. We define frames of minimal rotation (frames that do not rotate about their respective tangent axes along the backbone) at each point along the curve of each preshaped tube in its undeformed state $g_i^*(s) = \{R_i^*(s), p_i^*(s)\} \in \mathrm{SE}(3)$. The body frame "angular velocity" vectors (with respect to arc length rather than time) of these frames are then given by $\boldsymbol{\omega}_i^*(s) = (R^{*T}(s)\dot{R}^*(s))^\vee = \kappa_{xi}(s)\boldsymbol{e}_1 + \kappa_{yi}(s)\boldsymbol{e}_2$ where κ_{xi} and κ_{yi} are the curvatures in the x and y directions, and $\boldsymbol{e}_1, \boldsymbol{e}_2, \boldsymbol{e}_3 \in \mathbb{R}^3$ are the standard basis vectors. As set forth in [9], the $^\vee$ operator maps an element of $\mathfrak{so}(3)$ or $\mathfrak{se}(3)$ (the Lie algebras of $\mathrm{SO}(3)$ and $\mathrm{SE}(3)$, respectively) to its equivalent element of $\mathbb{R}^3$ or $\mathbb{R}^6$. The $\widehat{\ }$ operator denotes the inverse operation.

Now consider an arbitrary deformation of each tube consisting of bending and torsion with negligible shear and elongation, and let the tube curves and frames described above deform with the material so that $g_i(s) = \{R_i(s), p_i(s)\} \in \mathrm{SE}(3)$ describes the final shape of the i^{th} tube. Since these frames are defined by the deformation of the tubes, they will not correspond in general to the frames of minimal rotation for the deformed tube shapes.

The total elastic energy stored in these n deformed tubes is then the sum of the individual bending and torsional energy stored in each [12], [20],

$$E = \sum_{i=1}^{n} \underbrace{\frac{1}{2}\int_0^\ell \Delta\boldsymbol{\omega}_i^T(s) K_i(s) \Delta\boldsymbol{\omega}_i(s) ds}_{i^{\text{th}} \text{ tube energy}}, \tag{1}$$

where $\Delta\boldsymbol{\omega}_i(s) = \boldsymbol{\omega}_i(s) - \boldsymbol{\omega}_i^*(s)$, and $K_i(s) = \mathrm{diag}\{k_{i1}(s), k_{i2}(s), k_{i3}(s)\}$. In this paper, we consider cylindrical tubes of constant moment of inertia I and polar moment J. In this case, $k_{i1}(s) = k_{i2}(s) = E_i I_i$ and $k_{i3}(s) = G_i J_i$, where E denotes the elastic modulus and G the shear modulus. The active cannula shape will be a conformation that minimizes this stored elastic energy [20].

When the tubes are concentrically constrained, the $\boldsymbol{e}_3$ axes of all $R_i(s)$ must be equal. Without loss of generality, we let the first tube frame be a reference, writing $R_i(s) = R_1(s)\exp\left\{\widehat{\boldsymbol{e}}_3\theta_i(s)\right\}$ for $i = 2, \ldots n$. Therefore,

$$\boldsymbol{\omega}_i(s) = (R_i^T\dot{R}_i)^\vee = e^{-\widehat{\boldsymbol{e}}_3\theta_i(s)}\boldsymbol{\omega}_1(s) + \dot{\theta}_i(s)\boldsymbol{e}_3, \tag{2}$$

for $i = 2, \ldots n$. Substituting (2) into (1), and letting $\boldsymbol{\omega} = \boldsymbol{\omega}_1$, we complete the square (see [12] for an expanded description of the details) to obtain

$$E = \frac{1}{2}\int_0^\ell (\boldsymbol{\omega} - \boldsymbol{\alpha})^T K(\boldsymbol{\omega} - \boldsymbol{\alpha}) + C\, ds, \tag{3}$$

where,

$$\boldsymbol{\alpha} = K^{-1}(K_1\boldsymbol{\omega}_1^* + \sum_{i=2}^{n} K_i\overline{\boldsymbol{\omega}}_i^*),$$

$$C = \boldsymbol{\omega}_1^{*T}K_1\boldsymbol{\omega}_1^* + \sum_{i=2}^{n}\overline{\boldsymbol{\omega}}_i^{*T}K_i\overline{\boldsymbol{\omega}}_i^* - \boldsymbol{\alpha}^T K\boldsymbol{\alpha},$$

$$\overline{\boldsymbol{\omega}}_i^* = R_{\theta_i}\boldsymbol{\omega}_i^* - \dot{\theta}_i\boldsymbol{e}_3, \text{ and } K = \sum_{i=1}^{n} K_i.$$

Note that here $\boldsymbol{\alpha}$ and C are both functions of all θ_i and $\dot{\theta}_i$, and C is a strictly positive constant with respect to $\boldsymbol{\omega}$. In this form, it is clear that the choice of $\boldsymbol{\omega}$ which minimizes the integrand in a point wise sense is $\boldsymbol{\omega} = \boldsymbol{\alpha}$. Note that one can also arrive at this same result via applying the Euler–Poincaré equations or via a moment balance [12].

After substituting this result into (3), we convert the problem into a set of $n-1$ differential equations by applying the Euler–Lagrange equation,

$$\frac{\partial C}{\partial\theta_i} - \frac{d}{ds}\left(\frac{\partial C}{\partial\dot{\theta}_i}\right) = 0, \tag{4}$$

to the remaining integrand, C, $n-1$ times in order to find the functions $\theta_2, \ldots, \theta_n$ which correspond to a minimum energy conformation. Doing so yields a system of differential equations, namely,

$$(\boldsymbol{\alpha} - \overline{\boldsymbol{\omega}}_i^*)^T K_i\frac{\partial\overline{\boldsymbol{\omega}}_i^*}{\partial\theta_i} - (\dot{\boldsymbol{\alpha}} - \dot{\overline{\boldsymbol{\omega}}}_i^*)^T K_i\frac{\partial\overline{\boldsymbol{\omega}}_i^*}{\partial\dot{\theta}_i} = 0, \tag{5}$$

with $\theta_i(0) = \theta_{i0}$ and $\dot{\theta}_i(\ell) = 0$ for $i \in \{2, \ldots, n\}$. Solving these differential equations is the subject of the following section.

III. Solving for Cannula Shape

The expression (5) can be expanded in terms of precurvatures and stiffness matrices as follows,

$$\boldsymbol{e}_3^T \left(\sum_{j=2}^{n} \ddot{\theta}_j K_j K^{-1} - \ddot{\theta}_i \right) K_i \boldsymbol{e}_3 = \boldsymbol{\alpha}^T K_i \frac{\partial R_{\theta_i}}{\partial \theta_i} \boldsymbol{\omega}_i^* \quad (6)$$

In the case of $n = 2$ and constant curvature ($\boldsymbol{\omega}_i^* = \kappa_{xi} \boldsymbol{e}_1$) this expression reduces to the differential equation derived in [11]. Equation (6) can be reformulated into a format amenable to numerical integration by first writing it in matrix form as,

$$\ddot{\boldsymbol{\theta}} = \boldsymbol{T}^{-1} \boldsymbol{f}(\theta_2, \ldots, \theta_n), \quad (7)$$

Where $\boldsymbol{T} = \left[t_{i,j} \right]$ is an $n-1 \times n-1$ symmetric torsional stiffness matrix given by

$$t_{i,j} = \begin{cases} \frac{-J_{i+1} G_{i+1} \sum_{k=1, k \neq i+1}^{n} J_k G_k}{\sum_{k=1}^{n} J_k G_k} & i = j \\ \frac{J_{i+1} G_{i+1} J_{j+1} G_{j+1}}{\sum_{k=1}^{n} J_k G_k} & i \neq j \end{cases}. \quad (8)$$

Here,

$$\begin{aligned} \ddot{\boldsymbol{\theta}} &= \begin{bmatrix} \ddot{\theta}_2 & \ldots & \ddot{\theta}_n \end{bmatrix}^T, \text{ and} \\ \boldsymbol{f}(\theta_2, \ldots, \theta_n) &= \begin{bmatrix} f_1 & \ldots & f_{n-1} \end{bmatrix}^T, \end{aligned} \quad (9)$$

where,

$$f_i = \boldsymbol{\alpha}^T K_i \frac{\partial R_{\theta_i}}{\partial \theta_i} \boldsymbol{\omega}_i^*. \quad (10)$$

To write (7) in the form $\dot{\boldsymbol{x}} = f(\boldsymbol{x})$, one can augment the vectors on each side of the equation. Let $x_i = \theta_{i+1}$ for $1 \leq i \leq n-1$ and let $x_i = \dot{\theta}_{i-n+2}$ for $n \leq i \leq 2n-2$. The augmented first order system is then

$$\dot{\boldsymbol{x}} = \begin{bmatrix} \begin{bmatrix} x_n, x_{n+1}, \ldots, x_{2n-2} \end{bmatrix}^T \\ - - - - - - - - - - - - - \\ \boldsymbol{T}^{-1} \boldsymbol{f}(x_1, x_2, \ldots, x_{n-1}) \end{bmatrix}. \quad (11)$$

This system may now be solved with any of a number of numerical boundary value techniques that can accommodate mixed boundary conditions, for example Matlab's `bvp4c` function. Since all the tubes are the same length here, the boundary conditions will be $x_i(0) = \theta_{i+1}(0)$ for for $1 \leq i \leq n-1$ and $x_i(\ell) = \dot{\theta}_{i-n+2}(\ell) = 0$ for $n \leq i \leq 2n-2$.

A. Discussion

While the model described in Sections II and III is for a single section of overlapping tubes, it is straightforward to apply this to an active cannula with multiple regions of overlap, where tubes end at different arc lengths. One can consider each unique region of tube overlap (between arc lengths where tubes end) separately, with its own system of differential equations (11). Using a shooting method and enforcing continuity of boundary conditions at the junctions of these systems, one can compute the shape of the entire cannula. Note that this is equivalent to defining a new system similar to (11), but which is piecewise defined by the systems for each unique region of tube overlap.

Note that satisfying (7) is a necessary but not sufficient condition for $\boldsymbol{\theta}$ to correspond to a local minimum energy configuration, and that depending on the parameters, multiple solutions to (7) are possible. Thus the actual configuration of a physical cannula depends on configuration history. This phenomenon of multiple, history dependent, equilibrium states for the cannula has been observed in prototypes and accounted for in previous models [20]. As has been noted, these obstacles are surmountable in practical systems by using an approximate solution from previous servo cycle to initialize a numerical boundary value solver near the correct minimum. This is likely to work well at all points other than bifurcation points where the energy landscape structurally changes. Methods exist for predicting configurations where bifurcations occur in the case of two circular tubes [20], and it appears plausible that they may be generalizable to the multi-tube case also, although this is a topic we leave to future study.

B. Drawing the Backbone Curve

Once one has solved (11) numerically to obtain all $\theta_i(s)$ and $\dot{\theta}_i(s)$, the cannula shape is determined. There exist a number of numerical integration techniques that preserve the structure of $SE(3)$ [10], which can be used to obtain the backbone curve given $\boldsymbol{\omega}$. Here we follow a strategy that, while perhaps not optimal from an integration accuracy standpoint, is analogous to prior continuum robot results that parametrize the backbone in terms of curvature $\kappa(s)$ and bending plane $\phi(s)$. These are written in the "backbone frame," which is a frame of minimal rotation along the backbone. At the base of the cannula this frame aligns with the world frame. Each tube's reference frame differs from the cannula frame by a rotation of $\psi_i(s)$ about their common z axes, which can be found by,

$$\psi_i(s) = \psi_i(0) + \int_0^s \boldsymbol{\omega}_i^T(\sigma) \boldsymbol{e}_3 d\sigma. \quad (12)$$

Writing $\boldsymbol{\omega}_1$ in the cannula backbone frame, we have

$$\boldsymbol{\omega}_c = R_{\psi_1} \boldsymbol{\omega}_1 = \begin{bmatrix} \chi(s) & \gamma(s) & \boldsymbol{\omega}_1^T \boldsymbol{e}_3 \end{bmatrix}^{\mathrm{T}}, \quad (13)$$

where $\chi(s)$ and $\gamma(s)$ are the x and y components of curvature, respectively. This implies that $\kappa(s) = \sqrt{\chi(s)^2 + \gamma(s)^2}$ and $\phi(s) = \mathrm{atan2}(\gamma(s), \chi(s))$, where atan2 is the quadrant-specific arc tangent function. To draw the cannula as shown in all figures in the next section, we discretize $\kappa(s)$ and $\phi(s)$ at a large number of discrete arc length values, and apply the product of exponentials formula as given in [20].

IV. Example Case Studies

Here we apply the model developed in Sections II and III to several cannula configurations whose equilibrium conformation is somewhat intuitive. While our modeling framework can be be applied to much more complex configurations and precurvature functions, the illustrative examples selected here were chosen because 1) we believe them to lie near the limits of physical intuition, and 2) they are largely not possible to consider using prior models.

Figures 2, 3, and 4 each show a simulation of a three tube cannula where the tubes have equal constant curvatures,

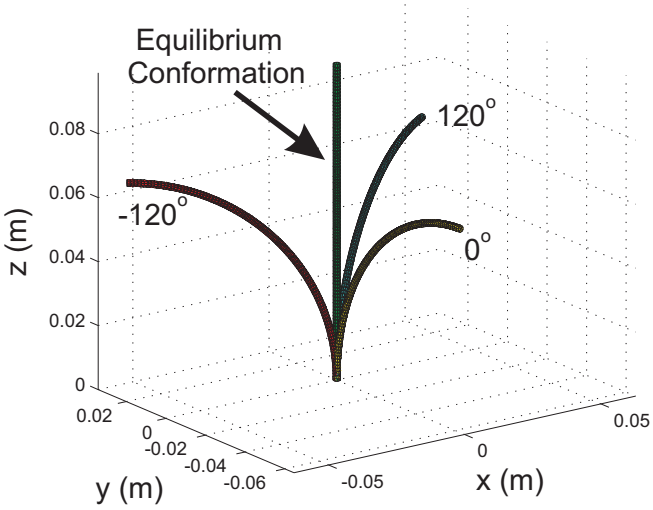

Fig. 2. The equilibrium conformation of three identical circular tubes spaced evenly at $0°$, $120°$, and $-120°$ is straight

stiffnesses, and lengths, all of which are similar to the physical prototype cannulas constructed in [20]. In Figure 2, the tubes are rotated to angles of $0°$, $120°$, and $-120°$. Our model predicts that the equilibrium conformation will be a straight cannula along the z axis, as shown in the figure. Note that this is a trivial solution of the model differential equation, since none of the tubes undergo any torsion.

In Figure 3 we simulate the three tubes described above, rotated to angles of $0°$, $60°$, and $-60°$. Our model predicts that the equilibrium conformation will lie in the plane of symmetry at $0°$. The tubes at $60°$, and $-60°$ undergo both bending and torsion as they conform, while the tube at zero degrees undergoes pure bending.

Figure 4 shows the result of the tubes rotated to angles of $90°$, $60°$, and $-45°$, illustrating a case where all tubes undergo bending and torsion simultaneously. The resulting equilibrium conformation lies in the expected location, namely between the $60°$ and $-45°$ tubes, but somewhat nearer the $60°$ tube. Note that the equilibrium conformation is also non-circular, agreeing with [11], which predicted a non-circular shape for 2 circularly precurved tubes when torsion was considered. Figure 5 shows the resulting torsional angles $\psi_1(s)$, $\psi_2(s)$, and $\psi_3(s)$ for the $90°$, $60°$, and $-45°$ tubes respectively. Note that the angles begin at base input values, and "relax" along the length of the cannula until their derivatives reach zero at its tip.

Lastly, we simulate two tubes with the same physical characteristics as in the previous examples, only with helical (rather than circular) precurvatures. One possible resulting shape is an intuitively pleasing circle in the plane of symmetry as shown in Figure 7. However there exists another, less intuitive equilibrium shape which is shown in Figure 6. Interestingly, the stored elastic energy is greater in the case of Figure 7 than in that of Figure 6.

V. Conclusion

In this work we have applied the framework of [12] to address the mechanics of both bending and torsional effects continuously along an active cannula composed of any number of arbitrarily curved component tubes. Such shapes are straightforward to achieve in physical tubes via heat treatment. Thus, it has not been manufacturing limitations, but rather modeling limitations, that have limited all prior active cannula prototypes to circular precurvatures. Arbitrary tube shapes have the potential to greatly extend the capabilities of active cannulas, enabling them to be much more dexterous with thinner diameters and/or fewer tubes than has been possible in the past. We believe that this model will facilitate future efforts toward moving active cannulas from the research laboratory into practical clinical settings.

Acknowledgement

This work was supported in part by the National Science Foundation under #CBET-0651803.

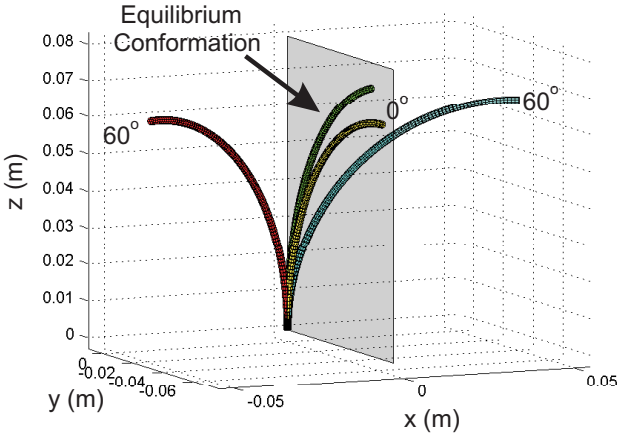

Fig. 3. The equilibrium conformation of three identical tubes rotated to $0°$, $60°$, and $-60°$ lies in the plane of symmetry at $0°$.

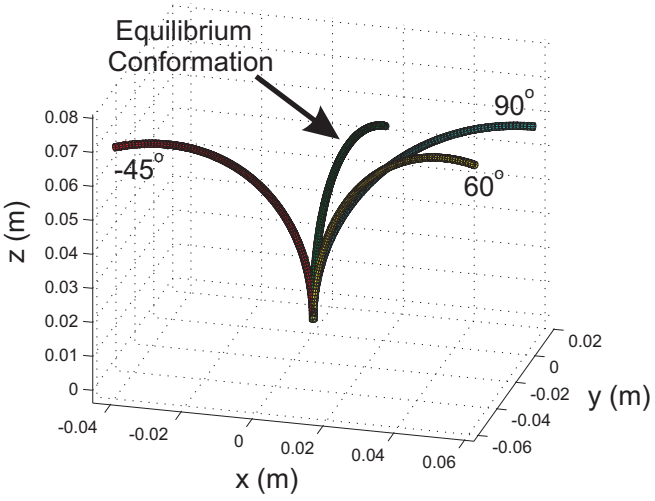

Fig. 4. The equilibrium conformation of three identical tubes, rotated to $60°$, $90°$, and $-45°$ is shown to be non-planar. All three tubes must undergo both bending and torsion in order to reach this configuration.

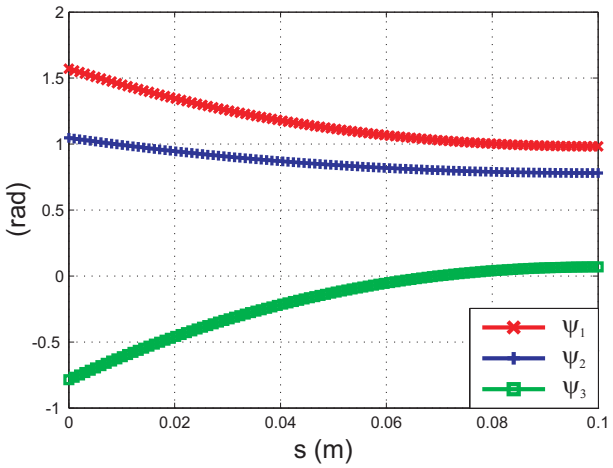

Fig. 5. Pictured are the torsional angles (12) for each tube for the simulation in Figure 4.

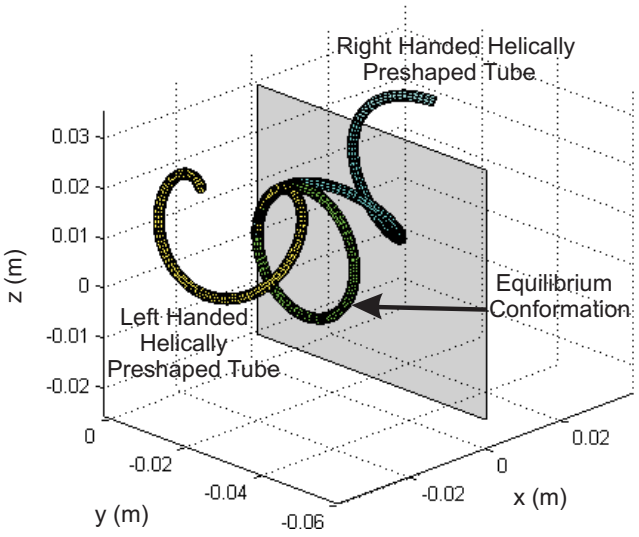

Fig. 6. One possible equilibrium conformation of two helically shaped tubes with equal stiffnesses.

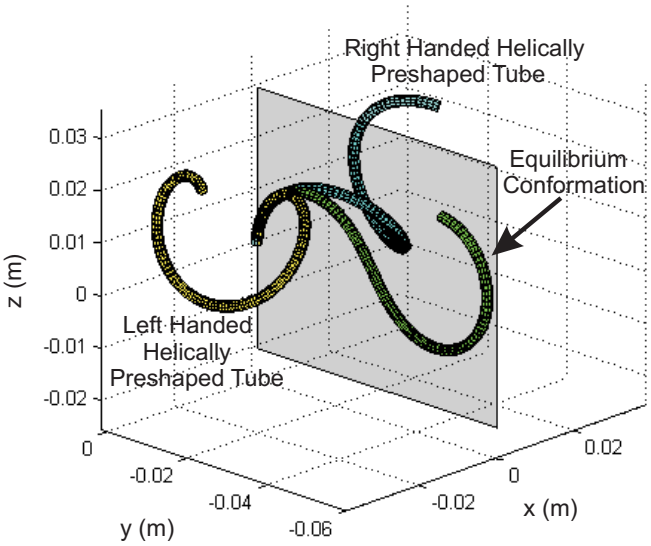

Fig. 7. Another possible equilibrium conformation of two helically shaped tubes with equal stiffnesses.

References

[1] R. Alterovitz, M. Branicky, and K. Goldberg. Constant-curvature motion planning under uncertainty with applications in image-guided medical needle steering. In *Workshop on the Algorithmic Foundations of Robotics*, July 2006.

[2] G. S. Chirikjian. Kinematic synthesis of mechanisms and robotic manipulators with binary actuators. *Journal of Mechanical Design*, 117:573–580, 1995.

[3] P. Dario, M. C. Carrozza, M. Marcacci, S. D'Attanasio, B. Magnami, and G. M. O. Tonet. A novel mechatronic tool for computer-assisted arthroscopy. *IEEE Transactions on Information Technology in Biomedicine*, 4(1):15–29, 2000.

[4] S. P. DiMaio and S. E. Salcudean. Interactive simulation of needle insertion models. *IEEE Transactions on Biomedical Engineering*, 52(7):1167–1179, July 2005.

[5] J. Furusho, T. Katsuragi, T. Kikuchi, T. Suzuki, H. Tanaka, Y. Chiba, and H. Horio. Curved multi-tube systems for fetal blood sampling and treatments of organs like brain and breast. *Journal of Computer Assisted Radiology and Surgery*, pages 223–226, 2006.

[6] M. W. Hannan and I. D. Walker. Kinematics and the implementation of an elephant's trunk manipulator and other continuum style robots. *Journal of Robotic Systems*, 20(2):45–63, 2003.

[7] B. A. Jones and I. D. Walker. Practical kinematics for real-time implementation of continuum robots. *IEEE Transactions on Robotics*, 22(6):1087–1099, Dec. 2006.

[8] M. Loser. A new robotic system for visually controlled percutaneous interventions under X-ray or CT-fluoroscopy. Master's thesis, The Albert-Ludwig-University, Freiburg, Germany, September 2002.

[9] R. M. Murray, Z. Li, and S. S. Sastry. *A Mathematical Introduction to Robotic Manipulation*. CRC Press, Boca Raton, FL, 1994.

[10] J. Park and W.-K. Chung. Geometric integration on euclidean group with application to articulated multibody systems. *IEEE Transactions on Robotics*, 21(5):850–863, 2005.

[11] D. C. Rucker and R. J. Webster III. Mechanics-based modeling of bending and torsion in active cannulas. *IEEE RAS/EMBS International Conference on Biomedical Robotics and Biomechatronics*, 2008. (In Press).

[12] D. C. Rucker, R. J. Webster III, G. S. Chirikjian, and N. J. Cowan. Equilibrium conformations of concentric-tube continuum robots. *International Journal of Robotics Research*, 2008. (In Review).

[13] P. Sears and P. E. Dupont. A steerable needle technology using curved concentric tubes. *IEEE/RSJ International Conference on Intelligent Robots and Systems*, pages 2850–2856, October 9-15 2006.

[14] N. Simaan, R. Taylor, and P. Flint. A dexterous system for laryngeal surgery. *IEEE International Conference on Robotics and Automation*, pages 351–357, 2004.

[15] I. Walker. Some issues in creating "invertebrate" robots. *Proceedings of the International Symposium on Adaptive Motion of Animals and Machines*, 2000. Montreal, Canada.

[16] R. J. Webster III. *Design and Mechanics of Continuum Robots for Surgery*. Mechanical engineering, Johns Hopkins University, Baltimore, MD, December 2007. PhD Thesis.

[17] R. J. Webster III, J. S. Kim, N. J. Cowan, G. S. Chirikjian, and A. M. Okamura. Nonholonomic modeling of needle steering. *International Journal of Robotics Research*, 25(5/6):509–526, May/June 2006.

[18] R. J. Webster III, A. M. Okamura, and N. J. Cowan. Toward active cannulas: Miniature snake-like surgical robots. *IEEE/RSJ International Conference on Intelligent Robots and Systems*, pages 2857–2863, October 9-15 2006.

[19] R. J. Webster III, J. M. Romano, and N. J. Cowan. Kinematics and calibration of active cannulas. *IEEE International Conference on Robotics and Automation*, pages 3888–3895, 2008.

[20] R. J. Webster III, J. M. Romano, and N. J. Cowan. Mechanics of precurved-tube continuum robots. *IEEE Transactions on Robotics*, 2008. (Accepted).

[21] R. J. Webster III, J. P. Swenson, J. M. Romano, and N. J. Cowan. Closed-form differential kinematics for concentric-tube continuum robots with application to visual servoing. *11th International Symposium on Experimental Robotics 2008, Springer Tracts in Advanced Robotics*, 2008. (In Press).